Kinetics of milk lipid droplet transport, growth, and secretion revealed by intravital imaging: lipid droplet release is intermittently stimulated by oxytocin

Andrius Masedunskas[a,b,†], Yun Chen[a,b,‡], Rebecca Stussman[a,b,§], Roberto Weigert[a,b,‖], and Ian H. Mather[a,b,c,‖,*]

[a]Laboratory of Cellular and Molecular Biology, Center for Cancer Research, National Cancer Institute, and [b]Intracellular Membrane Trafficking Section, National Institute of Craniofacial and Dental Research, National Institutes of Health, Bethesda, MD 20892; [c]Department of Animal and Avian Sciences, University of Maryland, College Park, MD 20742

ABSTRACT **The lipid droplet (LD) fraction of milk has attracted special attention because it supplies preformed lipids for neonatal development, and the assembled LDs are secreted by a unique apocrine mechanism. Because many aspects of this key process remain uncharacterized, we developed a facile method for the intravital imaging of mammary cells in transgenic mice that express fluorescently tagged marker proteins. Using these techniques, we describe the first kinetic analysis of LD growth and secretion at peak lactation in real time. LD transit from basal to apical regions was slow (0–2 μm/min) and frequently intermittent. Droplets grew by the fusion of preexisting droplets, with no restriction on the size of fusogenic partners. Most droplet expansion took several hours and occurred in apical nucleation centers, either close to or in association with the apical surface. Droplets even continued to expand as they were emerging from the cell. Contrary to expectations, LDs attached to the apical plasma membrane but still associated with the cytoplasm were released after oxytocin-mediated contraction of the myoepithelium. Thus milk LD secretion is an intermittently regulated process. This novel procedure will have broad application for investigating trafficking events within the mammary epithelium in real time.**

Monitoring Editor
Asma Nusrat
Emory University

Received: Nov 14, 2016
Revised: Jan 13, 2017
Accepted: Feb 1, 2017

This article was published online ahead of print in MBoC in Press (http://www.molbiolcell.org/cgi/doi/10.1091/mbc.E16-11-0776) on February 8, 2017.

[‖]Co–principal investigators.

Present addresses: [†]School of Medical Sciences, University of New South Wales, Sydney, NSW 2052, Australia; [‡]Department of Mechanical Engineering, Whiting School of Engineering, Johns Hopkins University, Baltimore, MD 21218, and Center for Cell Dynamics, School of Medicine, Johns Hopkins University, Baltimore, MD 21205; [§]Department of Mechanical Engineering, Columbia University, New York, NY 10027.

*Address correspondence to: Ian H. Mather (imather@umd.edu).

Abbreviations used: BODIPY, boron-dipyrromethene; GFP, green fluorescent protein; LD, lipid droplet; MSD, mean square displacement; rER, rough endoplasmic reticulum.

INTRODUCTION

Lactation is the defining physiology of mammals. All essential nutrients for the developing young, including lipid, protein, carbohydrates, and immune molecules, as well as water and ions, are supplied to the neonate from the lactating mammary gland during the first few days to years of life, depending on species (Oftedal, 1984; Oftedal and Iverson, 1995). Of these nutrients, milk lipid has attracted considerable attention because it is the sole source of preformed triacylglycerols, phospholipids, sphingolipids, sterols, fat-soluble vitamins, and long-chain polyunsaturated fatty acids, with the last named being essential for optimal postnatal brain development (Innis, 1991; Larque *et al.*, 2002).

Greater than 98% of the total fat-soluble material in milk comprises triacylglycerols, which are assembled and secreted in the form of membrane-coated lipid droplets (LDs). Although the biochemistry of triacylglycerol synthesis is firmly established

(Murphy, 2001), the mechanisms underlying LD assembly and secretion remain unclear (reviewed by Mather and Keenan, 1998; Heid and Keenan, 2005; McManaman *et al.*, 2007; McManaman, 2012). In the most widely accepted sequence of events, microdroplets of neutral lipid are assembled within the bilayer membrane of the rough endoplasmic reticulum (rER) and released into the cytoplasm coated with a monolayer of phospholipid derived from the cytoplasmic leaflet of the membrane (Mather and Keenan, 1998; Tauchi-Sato *et al.*, 2002; Martin and Parton, 2006; Wilfling, Haas, *et al.*, 2014). Droplets are then transported to the apical cytoplasm by poorly characterized mechanisms. Based on the analysis of electron micrographs, droplets in mammary cells either remain the same size or grow larger by fusion with each other (Dylewski *et al.*, 1984; Deeney *et al.*, 1985) and possibly by synthetic expansion in situ (Moriya, Uchida, *et al.*, 2011). During transit, LDs may interact with intracellular organelles, including the rER, mitochondria, Golgi membranes, and casein-containing secretory vesicles, before associating with the apical plasma membrane (Wooding, 1971; Peixoto de Menezes and Pinto da Silva, 1979; Wu *et al.*, 2000; Honvo-Houéto *et al.*, 2016). Droplets are then progressively extruded from the cell coated with an outer bilayer membrane derived from the apical surface (Bargmann and Knoop, 1959; Franke *et al.*, 1981; Mather and Keenan, 1998) and potential intracellular sources, most notably the outer membrane of casein-containing secretory vesicles (Wooding, 1971; Wu *et al.*, 2000; Honvo-Houéto *et al.*, 2016; Monks *et al.*, 2016). Finally, the completed droplets are released into luminal spaces by a poorly characterized "pinching-off" mechanism that is assumed to be continuous and constitutive.

This paradigm is based on classical biochemical and morphological approaches, using mammary homogenates and chemically fixed tissue that are limited by the lack of a kinetic dimension. Furthermore, analysis of milk secretion in vitro is not possible because there are no established cell lines that recapitulate the activities of terminally differentiated mammary cells in vivo. To surmount these barriers, we developed intravital imaging techniques for the lactating mammary gland using transgenic mice that express green fluorescent protein (GFP) or GFP-fusion proteins as morphological markers (Masedunskas *et al.*, 2014). We document the first measurements for rates of LD movement and assembly within the context of fully differentiated mammary cells in vivo and show that many of the mature droplets are intermittently expelled from the apical surface by oxytocin-mediated contraction of the myoepithelium.

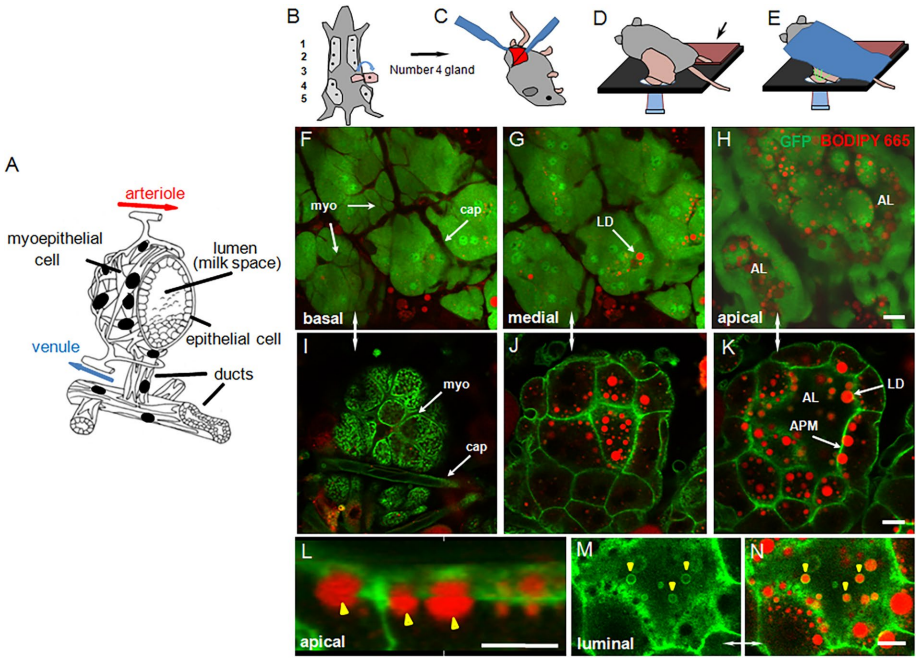

FIGURE 1: Intravital imaging of lactating mouse mammary gland. (A) Schematic of a mammary alveolus. The mammary epithelium is shown with associated capillary bed and a basal layer of myoepithelial cells, which forms a stellate basket-like structure around the alveolus. Milk collects in the central luminal (milk) space and on milk let-down is expelled into a system of ducts also lined with myoepithelial cells (modified from Gorden and Timms, 2004). (B–E) Preparation of number 4 mammary gland for intravital imaging. (B, C) Surgical preparation of skin flap with attached mammary gland and associated vasculature, (D) Positioning of the exposed gland on microscope stage, and (E) final position of mouse for imaging (for clarity, the Plexiglas stabilizer placed on top of the gland is not shown). (F–N) In situ BODIPY-labeled intravital confocal sections of lactating mammary gland from (F–H) the GFPcyto mouse, showing optical sections through the basal, medial, and apical regions of the secretory epithelium (the myoepithelium and capillary endothelial cells appear dark because of their relative lack of GFP compared with the secretory epithelium); (I–N) the GFP-membrane mouse, showing (I–K) basal, medial, and apical regions of the secretory epithelium with targeting of GFP to apical, lateral, and basal plasma membranes, (L) 3D reconstruction of secretory epithelial cells showing accumulation of LDs (yellow arrowheads) under the apical plasma membrane, (M, N) an *en face* section across the luminal side of the apical surface showing LDs (yellow arrowheads) emerging from the cell; (M) GFP, and (N) combined GFP and BODIPY 665/676. BODIPY-stained LDs are shown in red and GFP in green. AL, alveolar lumen; APM, apical plasma membrane; cap, capillary; LD, lipid droplet; myo, myoepithelial cell. Bars, 20 μm (F–H), 10 μm (I–N).

RESULTS

Introduction to mammary cell architecture and the experimental system

Milk is synthesized in polarized epithelial cells, which are organized into alveoli and enveloped by a myoepithelium on the basolateral side (Figure 1A). The entire structure is stabilized by a basement membrane that coats the outer surface (not shown). Blood-borne precursors are supplied from a capillary bed and taken up across basal/lateral membranes into the secretory epithelium. Completed milk products are secreted from the apical surface into a central alveolar lumen. Alveolar units are typically 100–150 μm in diameter and may expand or contract, depending on the amount of milk stored in luminal spaces. Using intravital laser scanning confocal microscopy (Weigert *et al.*, 2013), we obtained *Z*-stack, or time-lapse, images to a depth of ~15–20 μm, capturing the top portion of the alveoli. This distance was sufficient to encompass the extracellular matrix, associated adipocytes, and capillary bed, one layer of myoepithelial and secretory epithelial cells, and the most proximal portion of the central cavity.

The number 4 glands of either GFPcyto or GFP-membrane mice were prepared for imaging as described in *Materials and Methods* (Figure 1, B–E). General tissue architecture and intracellular structures were manifest to a high resolution in both transgenic strains. In the GFPcyto mouse, GFP is

ubiquitously expressed as a soluble protein at varying levels within and between cell types (Hadjantonakis *et al.*, 1998). Most milk-secreting cells were intensely fluorescent, GFP filled the cytoplasm, and nuclei were obvious. In contrast, both the myoepithelium and capillary bed were distinguished by their relative lack of fluorescence compared with the secretory epithelium (Figure 1, F–H). Boron-dipyrromethene (BODIPY)–stained LDs were identified as round, fluorescent objects of variable size throughout the cell, with the larger droplets concentrated in the apical cytoplasm and abutting the apical surface.

In the GFP-membrane mouse, GFP is targeted to the plasma membranes of most cells by a prenylated peptide derived from the MARCKS protein fused to the N-terminus (Mazumdar *et al.*, 2007). GFP decorated all surfaces of capillary endothelial cells, circulating leucocytes, the myoepithelium, and secretory epithelium (Figure 1I). Within the secretory epithelium, the deeply infolded basal plasma membrane and lateral and apical surfaces were clearly delineated in confocal sections through a depth of ~20 µm (Figure 1, I–K). Association of the larger BODIPY-stained LDs with the apical surface was clear from both single confocal sections and three-dimensional (3D) reconstructions (Figure 1, K and L). In favorable grazing sections, LDs could be identified emerging from the cell coated with GFP-labeled membrane (Figure 1, M and N).

There was little evidence of surgery-induced inflammation within the 3- to 4-h imaging time frames employed. Diapedesis of neutrophils was not observed, and there was no evidence of vasodilation of the capillary bed or obvious tissue damage. Macrophages were evident as relatively dark mobile cells, which infiltrated the interstitial spaces underlying the secretory epithelium in both transgenic lines. Their presence was to be expected, as they are well-characterized residents of the gland that are essential for mammary development during pregnancy and for the maintenance of the differentiated state throughout lactation (Gouon-Evans *et al.*, 2002; Reed and Schwertfeger, 2010). Furthermore, in rodents, they constitute the most abundant cell type in milk from disease-free glands (Head and Beer, 1978).

LD transport and fusion

BODIPY-stained LDs in secretory epithelial cells were assessed with respect to their size, location in the cell, and rate and direction of transport in movies over periods of 1–2 h. Short-term movement (5–10 s) was measured using a custom-written program in Matlab software. Longer-term movement was manually tracked in the most stable areas of the movies for up to 30 min. Mobile LDs were identified with diameters between 0.7 and >8 µm (Figure 2A), a size range that encompasses ~60% of the LDs identified in chemically fixed glands (Supplemental Figure S1A) and accounts for the bulk of LD volume (Supplemental Figure S1B). The most abundant LDs analyzed had diameters between 1 and 3 µm (1.89 ± 0.33 µm; Table 1). Because of limits in intravital resolution, we were unable to monitor the earliest stages of LD formation when nascent micro-LDs <250 nm in diameter (Kassan *et al.*, 2013) assemble within the hydrophobic core of the rER. Resolution issues also precluded the analysis of LDs <0.5 µm in diameter that are directly secreted into milk (Dylewski *et al.*, 1984; Deeney *et al.*, 1985). Such droplets comprise the largest proportion in terms of number but contribute a negligible amount to total milk-lipid volume (Figure S1, C and D). With these caveats in mind, analysis of movies from three mice yielded consistent data with respect to LD size, speed, and cellular location (Table 1; individual mice color coded in Figure 2, A–C).

There was a pronounced polarized distribution with respect to size, with the largest droplets in the cell apex, many of which were associated with the apical surface (Figures 1, K and L, and 2A). Many such droplets were in the process of budding from the cell and were >4.0 µm in diameter. They were also the most infrequent, accounting for <7% of the total measured. The largest droplets were in the same size range as the large LDs in expressed milk, the latter of which had mean diameters of from 4–10 µm (Supplemental Figure S1C) and accounted for >70% of the total volume of milk lipid (Supplemental Figure S1D). This distribution profile was largely in agreement with measurements from chemically fixed glands (Supplemental Figure S1, A and B) and emphasized the directional growth of droplet size and decreased abundance in moving from the basal to apical cytoplasm.

BODIPY-stained lipid droplets within the cell interior were either intermittently stationary or moved with variable speeds toward the cell apex in a basal-to-apical direction (example of vector map in Figure 2D and Supplemental Videos S1–S4.mov). The short-term speeds measured over 5 or 10 s were in the range 2.46 ± 0.77 µm/min (Table 1) and largely reflected oscillatory thermal motion (examples of mobile and stationary LDs in Supplemental Figure S2, A–D and E–H, respectively). Average forward speeds measured up to distances of 10 µm were highly variable, ranging from 0.02 to 4.7 µm/min with 75% of the measured droplets moving at <1 µm/min (0.72 ± 0.09 µm/min; Table 1 and Figure 2B). When stationary droplets and intermittent pauses in the trajectories of mobile LDs were excluded from the analysis, the average speed was ~100% higher (1.55 ± 0.43 µm/min; Table 1).

There was no obvious correlation between LD size and speed, except that droplets >~2.5 µm in diameter were essentially stationary (Figure 2C), and most of these were in close proximity to the apical plasma membrane (Figure 2A). Small LDs appeared to arise from within the depth of the cell in areas shown by electron microscopy to be rich in rER (Bargmann and Knoop, 1959; Wooding, 1977), and they moved at variable rates toward the apical surface, although stationary droplets were seen throughout the cell (Figure 2, B and C). Many active droplets were observed within the apical cytoplasm above the nucleus (≤7 µm from the apical plasma membrane; Figure 2B), and there was a significant decrease in average speed as the droplets approached the surface (inset, Figure 2B).

LD motion was further characterized by plotting the mean square displacement (MSD) and frame-by-frame diffusion coefficient (*D*; see *Materials and Methods* for definitions) against time intervals for each of the 300 tracked droplets. Droplet movements fell into one of three broad categories: 1) *diffusive*, in which there was a linear increase in MSDs, but values for *D* remained constant (Figure 3, A and B); 2) *directed* (*superdiffusive*), in which there was an additional nonlinear component accounting for fast increases in MSD values (Figure 3, C and D); and 3) *mixed*, in which droplets displayed both kinds of motion (Figure 3, E and F). About half of LDs in all three mice were directed (Table 1 and Supplemental Figure S3), but there was a decrease in their total percentage toward the cell apex and a compensatory increase in droplets exhibiting typical diffusive behaviors (Figure 3G). Many of the latter droplets were closely associated with the apical surface. Surprisingly, none exhibited confined motion, which might be expected of LDs partially immobilized by attachment to an outer plasma membrane layer, suggesting that this outer layer is itself dynamic. As expected, there was a significant increase in the percentage of droplets throughout the cell with directed motion (from 50.92 ± 3.78 to 74.98 ± 6.28%) and an increase in the average values for *D* (from 0.085 ± 0.021 to 0.104 ± 0.029 $\mu m^2/s$; Table 1) when only the most extensive contiguous mobile portion of each track was analyzed (Figure 3H and Supplemental Figure S3). Thus the motion of a majority of the droplets, for at

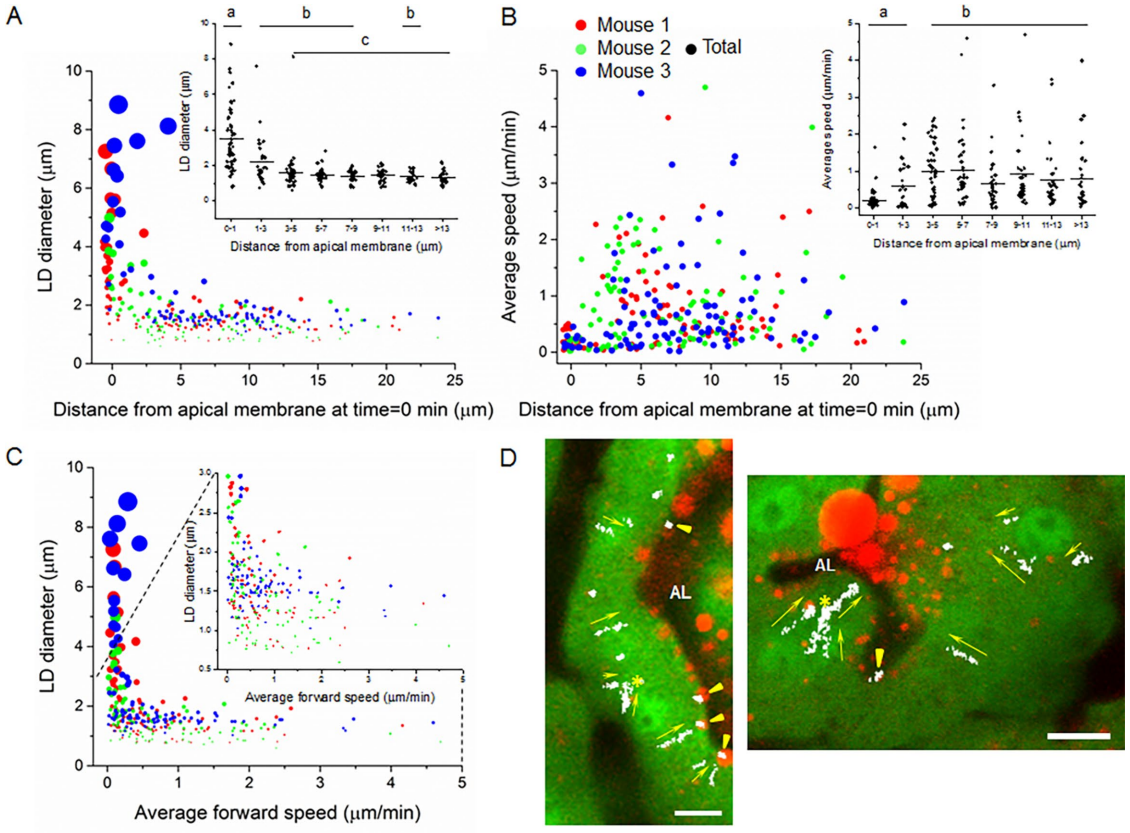

FIGURE 2: Kinetic analysis of LD movement in GFPcyto mouse mammary cells. Manually tracked data points from three mice are color coded and proportionally adjusted to indicate relative LD volumes (A, C). (A) Relationship between LD diameter and distance from the apical surface at the beginning of each track. Inset, binned data for all three mice. Mean values labeled with different letters are significantly different from each other, $p \leq 0.05$ (pairwise comparison using Tukey and Kramer test). (B) Relationship between average LD speed and distance from the apical surface at the beginning of each track. Inset, binned data for all three mice. Mean values labeled with different letters are significantly different from each other (pairwise comparison using Tukey and Kramer test), $p < 0.05$. (C) Relationship between LD diameter and average forward speed. Inset, enlarged area encompassing LDs ≤3 μm in diameter. (D) Vector map showing the direction (yellow arrows) of LD movement in representative movies. Examples of mobile and stationary LDs are indicated by yellow arrows and arrowheads, respectively, and points of LD fusion by yellow asterisks. AL, alveolar lumen. Bars, 10 μm (D).

least a portion of the trajectories, was directed until the LDs approached and engaged with the apical surface.

Droplets grew by fusing together at all positions in the cell (Figure 4, A–D, Supplemental Figure S4, and Supplemental Videos S1–S4.mov) with no obvious size restrictions on fusogenic partners. Small droplets fused with small, medium, or large droplets, and large droplets fused with each other (Figure 4B and Supplemental Video S2.mov; see, e.g., examples of large droplets fusing with each other [from 0 min to 48 min, 50 s], a medium-sized droplet fusing with a large droplet [from 30 min to 44 min, 30 s], and small droplets fusing with each other in the vicinity of a large droplet [from 76 min to 80 min, 10 s]). Many droplets within the depth of the cell appeared to move on defined pathways or tracks and sometimes fused together by "catching up" with each other during transit (Figure 4, A, C, and D, and Supplemental Videos S1.mov, S3.mov, and S4.mov). Droplets grew most noticeably in the cell apex, especially after they had engaged with the apical plasma membrane (Supplemental Videos S2–S4.mov). In some cases, the origin of these "apical nucleation centers" could be traced to the delivery of single small droplets (<1 μm) to the apical surface, which then served as assembly points for the progressive fusion of additional droplets that often followed the same trajectory to the surface (arrowheads and white square brackets, Figure 4C and Supplemental Video S3.mov; blue arrowheads and square brackets, Figure 4D and Supplemental Video S4.mov). Droplet expansion continued even as they were emerging from the cell (white arrowheads and dotted enclosure, Figure 4D, Supplemental Figure S5, and Supplemental Video S4.mov).

The final assimilation of one droplet into another varied from a few seconds to prolonged periods. In some cases, even after droplets appeared to be in close contact with each other, the complete assimilation step took up to 30 min (Figure 4, B–D, final assimilations denoted by green arrows; Supplemental Videos S2–4.mov and Supplemental Figure S4). The final mixing of lipids was unidirectional even when the droplets were of equal size (Figure 4E), suggesting that fusion was mediated by a specific vectorially based mechanism.

Release of droplets

After completion of LD formation, droplets coated with an external bilayer membrane are released from the cell by a "pinching-off" mechanism in which the remaining narrow neck of apposing

Parameter	Mouse number			Mean ± SD
	1	2	3	
1) Program				
Number of cells	27	27	30	
Number of measurements	2568	1448	606	
Average short-term speed (+/–) (μm/min)	1.62 ± 1.42	2.62 ± 1.89	3.15 ± 2.55	2.46 ± 0.77
2) Manually tracked LDs				
(a) Total				
Number of cells	27	18	25	
Number of LDs	103	95	102	
LD diameter (μm)	1.95 ± 1.24	1.53 ± 0.76	2.18 ± 1.59	1.89 ± 0.33
Average forward speed (μm/min)	0.63 ± 0.71	0.82 ± 0.84	0.72 ± 0.82	0.72 ± 0.09
Directed motion (%)	50.48	47.37	54.9	50.92 ± 3.78
Average *D* ($\mu m^2/s$)	0.062	0.104	0.089	0.085 ± 0.021
(b) Unimpeded LDs				
Number of cells	27	18	25	
Number of LDs	58	57	73	
LD diameter (μm)	1.36 ± 0.37	1.21 ± 0.35	1.59 ± 0.32	1.39 ± 0.19
Average unimpeded forward speed (μm/min)	1.24 ± 0.93	2.04 ± 2.11	1.37 ± 1.12	1.55 ± 0.43
Directed motion (%)	81.03	75.43	68.49	74.98 ± 6.28
Average unimpeded *D* ($\mu m^2/s$)	0.076	0.135	0.102	0.104 ± 0.029

Data in the far right column are calculated from the individual means for mice 1, 2, and 3.

TABLE 1: LD parameters and estimates for average LD speed.

membrane undergoes sequential fusion and fission steps. In the currently accepted paradigm, this terminal step is assumed to be continuous and constitutive. Therefore we were surprised that in the analysis of >20 movies from different transgenic mouse strains, we never observed complete release of a single large LD. Even droplets that were maximally protruding from the apical surface remained associated with the cell within the feasible ≤2-h imaging times used.

The nonapeptide hormone oxytocin is released from the pituitary gland into the peripheral blood in response to stimulation of afferent nerves in the nipple (Gimpl and Fahrenholz, 2001). Subsequently, blood-borne oxytocin binds to a G protein–coupled receptor on the myoepithelial cell surface, leading to actin-based contraction of the myoepithelium, collapse of the alveoli, and expulsion of secreted milk from luminal spaces (the so-called "milk let-down reflex"). In several trial experiments, oxytocin was injected intraperitoneally to assess its effect on the distribution of LDs that had accumulated in the cell apex. Within 1–2 min after injection, oxytocin induced periodic contractions of all alveoli, which were recorded by intravital imaging for up to 20 min (Supplemental Video S5.mov). Comparison of single optical sections and 3D reconstructions before and after treatment showed almost complete removal of LDs from luminal spaces and the apical surface (Figure 5, A–D), including many droplets that were still partly associated with the cytoplasm (example, white arrowheads, Figure 5, A and B). This result suggested that oxytocin not only functions to expel secreted LDs from luminal spaces (the classical paradigm) but that it also induces release of LDs associated with the cell, that is, LD *secretion* is intermittently stimulated by milk let-down.

We therefore asked whether expulsion of LDs is dependent on oxytocin in animals that have not been subjected to any surgical manipulation, in order to eliminate potential experimental artifacts associated with anesthesia, surgical procedures, or the nonphysiological application of oxytocin by intraperitoneal (i.p.) injection. The distribution of LDs at the apical surface that were *still in partial contact with the cytoplasm* was measured by quantitative morphometry of mammary glands from two groups of lactating GFPcyto mice that were either immediately killed by intracardiac fixation (control) or separated from their litters for 4 h before fixation and analysis (test; see Supplemental Figure S6 for explanation of the method used). If LD secretion is a continuous process, there should be no difference in the amount of apical lipid in partial contact with the cytoplasm before or after litter separation. However, after 4 h, there was a 3.5-fold increase in the volume of apical lipid in the test group compared with the control (Figure 5, E–H and K, and Supplemental Figure S7). In a further group, mothers were separated from their litters for 4 h and then injected with oxytocin. Apical lipid amounts were reduced to the levels measured in the 0-h controls (Figure 5, I–K, and Supplemental Figure S7). These data are consistent with a mechanism for the terminal release of LDs mediated through oxytocin-induced contractions of the mammary alveolus, even for those droplets still in the process of budding from the cell.

Finally, we used the foregoing assay to measure the rate of accumulation of apical lipid during intravital imaging by comparing 3D reconstructions of the imaged area recorded just before and immediately after imaging four mice (1-h movies each). The amount of apical lipid in droplets *still partly associated with the cytoplasm* averaged 61.95 ± 20.67 μm^3/cell/h, which was nominally higher than the value of 23.7 ± 1.87 μm^3/cell/h obtained from measurements in

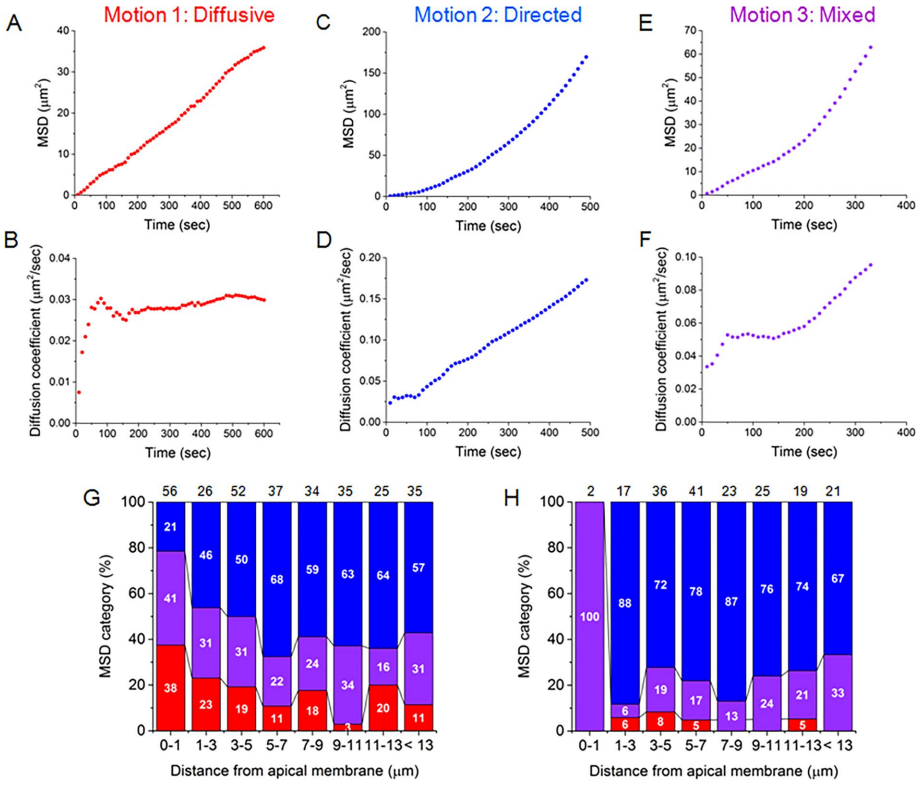

FIGURE 3: Classification of LD movement according to measurements of MSD and frame-by-frame values for *D*. Examples of MSD vs. time plots of (A, B) diffusive motion, (C, D) superdiffusive directed motion, and (E, F) mixed motion. Mode of transport (binned %) as a function of distance from the apical surface for (G) complete trajectories (300 LDs) and (H) a subset of trajectories of mobile LDs in which only the most extensive contiguous mobile portion of each track was analyzed (184 LDs). Motion categories are color coded as in A–F. The total number of droplets and distribution (%) of each motion category within each bin are indicated by black numbers above and white numbers within each column, respectively.

fixed glands after allowing lipid to accumulate for 4 h in vivo (calculated from the data in Figure 5K). The approximate concordance between these values obtained under similar assay conditions provides some reassurance that the intravital measurements were not compromised by the surgical procedures and imaging techniques, given the limited number of cells (total of 75) that were assayed during intravital imaging compared with the number assayed in vivo (total of 1816 cells in the 0-h and 1511 cells in the 4-h controls). Using the most reliable literature values for the peak quantities of milk produced in lactating mice (Knight *et al.*, 1986), we estimate that mammary cells secrete ~70 μm^3 lipid/cell/h (Supplemental Data, Supplemental Table S1, and Supplemental Figure S8). This secretion rate is qualitatively in line with the foregoing experimental values, keeping in mind that only the volume of lipid in droplets still in contact with the apical cytoplasm was assayed through a depth of 10 μm, that is, a proportion of the total apical lipid in less than one whole cell.

DISCUSSION

This study reveals novel insights into the assembly and secretion of milk lipid droplets in vivo. On a kinetic basis, the process can be separated into four stages: 1) the slow, directed intermittent transport and expansion of LDs on potential tracks from basal sites of synthesis to the cell apex (Figure 6A), 2) further LD expansion in the apical cytoplasm before, during, and after engagement with the plasma membrane (Figure 6, B–D), 3) continued expansion of LDs as they emerge from the cell (Figure 6E), and 4) oxytocin-mediated rapid release of LDs still partially associated with the cytoplasm (Figure 6F). Because of limits in optical resolution, we were unable to estimate the number of LDs released by oxytocin that were in the absolute final stages of secretion or droplets that may have emerged from the cell and been adsorbed to the outer apical surface. These were droplets for which there was no discernible contact between the BODIPY-stained lipid and the GFP-labeled cytoplasm (Figure 6G and Supplemental Figure S6). Neither could we analyze droplets that may be secreted with minimal enlargement by a pathway first described by Dylewski *et al.* (1984) and Deeney *et al.* (1985) (Figure 6H) because LDs <0.7 μm were not well detected for extended imaging times with our intravital microscopy system.

Many of the smaller LDs within the depth of the cell appeared to move on the same pathway or track as they migrated to the apical surface (Figure 4, A, C, and D) and exhibited directed (superdiffusive) behavior. Superdiffusion is an anomalous form of diffusion in which lateral mobility is augmented by directed motion and is one form of diffusive behavior associated with the movement of particles through a viscous and organelle-rich cytoplasm (Caspi *et al.*, 2000). Examples include the recruitment and transport of secretory vesicles on microtubules and actin filaments in chromaffin cells (Maucort *et al.*, 2014) and transport of vesicles and granules by myosin II motors in *Acanthamoeba castellanii* (Reverey *et al.*, 2015). Thus the superdiffusive character of LDs in mammary cells is consistent with their directed transport to the cell apex on elements of the cytoskeleton.

In some cell types, LDs are transported rapidly on microtubules (Welte, 2009), and in mammary cells, dynein motors (Wu *et al.*, 2000) may drive droplets toward the centriole, which is close to the apical surface (Dylewski and Keenan, 1984). However, the average speeds measured in this study were slow (<1–2 μm/min; Table 1), that is, <1–2% of those for LDs moving on microtubules in *Drosophila* embryos (>1.0 μm/s; Welte, Gross, *et al.*, 1998) and in HuH7 cells (2.0–2.5 μm/s; Targett-Adams *et al.*, 2003). Several factors may underlie these differences. Unlike many systems, a proportion of the LDs in mammary cells actively expand by progressive fusion reactions of precursor LDs (Figure 4). The rate of LD movement may also be affected by interactions with other organelles, including documented interactions with the rER, mitochondria, Golgi-derived secretory vesicles, and potential endosomes (Wooding, 1971; Wu *et al.*, 2000; Mather *et al.*, 2001; Honvo-Houéto *et al.*, 2016). On the other hand, attempts to suppress lipid secretion with microtubule inhibitors in a number of experimental contexts have yielded conflicting and ambiguous results (discussed in Mather and Keenan, 1998; Heid and Keenan, 2005).

The possibility that LDs are transported on other elements of the cytoskeleton, including actin cables, deserves special attention (Amato and Loizzi, 1981; Heid and Keenan, 2005; Welte, 2009).

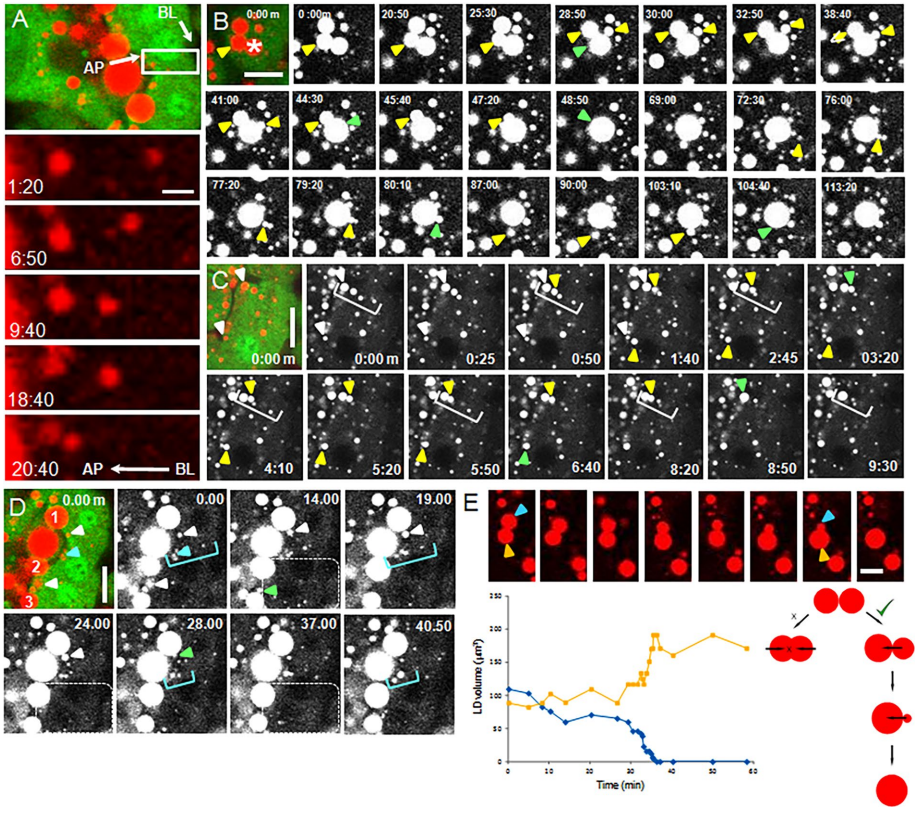

FIGURE 4: Fusion of LDs during intracellular transit. (A) Movement of an LD from basal to apical regions over a period of 20 min (white boxed area) showing progressive fusions with other LDs during transit (Supplemental Video S1.mov). AP, apical plasma membrane; BL, basal plasma membrane. (B) Fusion of both large LDs (3–4 μm) with each other, small LDs (≤1 μm) fusing with large LDs, and small LDs fusing with each other in the vicinity of large LDs (yellow arrowheads; points of fusion denoted by green arrowheads; Supplemental Video S2.mov). See Supplemental Figure S4 for graph of the droplet cluster marked with an asterisk. (C) Small LDs at the apical surface (white arrowheads) serve as nucleation centers for the fusion of additional LDs (yellow arrowheads), some of which appear to follow tracks to the surface (white brackets; points of fusion are marked by green arrowheads; Supplemental Video S3.mov). (D) LDs continue to expand by fusion with smaller LDs even when they are protruding from the apical surface. Three large LDs (1–3) receive additional lipid from smaller LDs at the apical surface (white arrowheads; points of fusion marked by green arrowheads) and from small droplets coming from the depth of the cell (area enclosed by dotted line). An additional small LD (blue arrow) serves as a nucleation center for droplets on a presumptive track to the apical surface (blue brackets; see Supplementary Figure S5 for a 3D analysis of this region; Supplemental Video S4.mov). (E) Mixing of lipid after fusion is unidirectional even when the LDs are approximately the same size (orange and blue arrowheads and lines indicate LDs in the micrographs and lipid volumes in the plots, respectively). LD volume was estimated from LD areas in two dimensions. Schematic to the right differentiates between equal (x) and unidirectional mixing (√). (A–D) Initial frames are shown with BODIPY-stained LDs in red and cytoplasmic GFP in green. Bars, 2 μm (A), 10 μm (B–E). All videos, 10 μm.

Actin and myosin II inhibitors disrupt LD movement in zebrafish embryos (Dutta and Sinha, 2015), and LDs in *Saccharomyces cerevisiae* segregate into the growing bud through the action of Myo2p at speeds comparable to those for mammary LDs, that is, between 1.8 and 3.0 μm/min (Knoblach and Rachubinski, 2015). Unfortunately, attempts to inhibit LD secretion in vivo with cytochalasin B were compromised by collapse of the myoepithelium and loss of alveolar structure (unpublished data). In future experiments, these issues may be resolved through intravital imaging of transgenic mouse strains in which gene sequences for fluorescent reporter proteins are "knocked into" genes encoding specific components of the transport machinery.

Our intravital images confirm that LDs grow through the progressive fusion of precursor LDs, especially in the apical cytoplasm. We saw no evidence for the rapid expansion of individual LDs (>0.7 μm diameter) in the absence of discrete cytoplasmic BODIPY-stained precursors, for example, through the activity of lipid synthetic enzymes in situ (Fujimoto *et al.*, 2007; Moriya, Uchida, *et al.*, 2011) or evidence for the fragmentation of preexisting droplets, that is, droplet expansion appeared to be a unidirectional process. Despite claims to the contrary (Stemberger and Patton, 1981; Dylewski *et al.*, 1984; Heid and Keenan, 2005), LD fusion was not limited to small LDs fusing with large droplets. There was no restriction on the size of fusogenic partners, to the extent that LDs >2–3 μm in diameter fused with each other (e.g., Figure 4B and Supplemental Figure S4).

LDs did not mix equally; instead, one droplet was completely subsumed by the other, even when they were approximately of the same size (example in Figure 4E). Such vectorially directed mixing reactions are strikingly similar to the slow fusion of LDs in 3T3-L1 cells (Gong, Sun, *et al.*, 2011) and brown adipocytes (Barneda *et al.*, 2015), in which members of the Cide family mediate droplet fusions through the formation of interactive dimers (compare Figure 4E of this study with Figure 1 of Barneda *et al.* (2015)). CideA is the most likely fusogenic partner in mammary cells, as knockout of the *CideA* gene in mice disrupts lipid secretion (Wang *et al.*, 2012), and it is enriched at LD contact sites (Monks *et al.*, 2016). Mammary cells provide an alternative model system for studying the role of CideA and other constituents in droplet growth because the fusion of LDs is a relatively rare event in many cells (Suzuki *et al.*, 2011).

Final contact between the plasma membrane bilayer and droplet surface is mediated through the integral protein butyrophilin (Jack and Mather, 1990; Ogg *et al.*, 2004), which forms an oligomeric secretion complex with xanthine oxidoreductase (Jeong, Rao, *et al.* 2009; Monks *et al.*, 2016), plin-2 (adipophilin), and other proteins on the droplet surface (Chong *et al.*, 2011; McManaman, 2012; Jeong, Lisinski, *et al.*, 2013). Thus, regardless of initial droplet size, further expansion should continue with progressive recruitment of more xanthine oxidoreductase and butyrophilin molecules as the droplets emerge from the cell (Monks *et al.*, 2016).

In the absence of oxytocin, formation of mature LDs may last several hours. During this time, expansion by consecutive fusion reactions continues even when a substantial proportion of the lipid is protruding into luminal spaces (e.g., Figure 4D and Supplemental Figure S5), a mechanism that was predicted from quantitative morphometry of fixed tissue >35 yr ago (Stemberger and Patton, 1981;

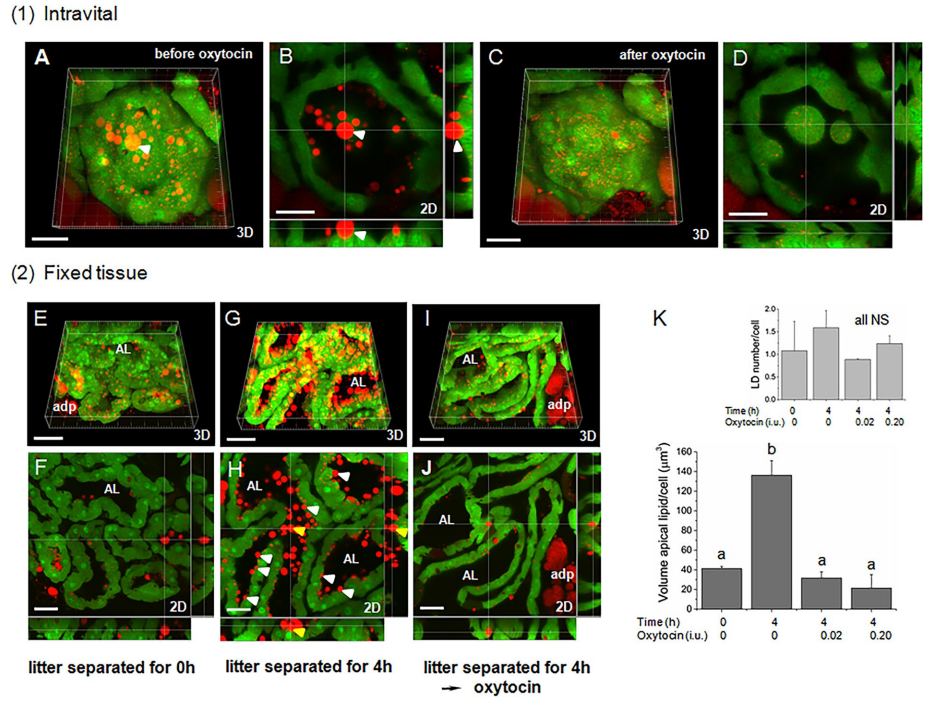

FIGURE 5: Final release of LDs from the apical surface is mediated by oxytocin-induced myoepithelial cell contractions. (A–D) Intravital alveolar contractions induced by the i.p. injection of 0.02 IU oxytocin (Supplemental Video S5.mov). (A, B) before oxytocin, (C, D) after oxytocin; 3D (A, C), and 2D sections (B, D) of same alveolus before and after oxytocin. Note loss of LDs from the apical surface, including at least one embedded in the cytoplasm (white arrowhead). (E–J) Representative micrographs of mammary glands from groups of GFPcyto mice (four animals/group), which were (E, F) perfusion fixed immediately after separation from their litters (0-h control), (G, H) separated from their litters for 4 h before sacrifice (4 h control), or (I, J) separated from their litters for 4 h before injecting with either 0.02 IU oxytocin (2 mice; oxytocin 0.02 test) or 0.2 IU oxytocin (2 mice; oxytocin 0.2 test) and then perfusion fixing of mice 20 min later (example shown after 0.02 IU). Note accumulation of LDs at the apical surface after 4 h in G and H and their release after treatment with oxytocin in I and J. A few examples of LDs still embedded in the cytoplasm are indicated by white arrowheads, including one that in cross section (H) appears to be free in the AL (yellow arrowhead); 3D (E, G, I), and 2D sections (F, H, J). (K) Quantitative data from experiment in E–J. Inset, LD numbers/cell analyzed for each treatment. Mean values (± SD) labeled with different letters are significantly different from each other; $p \leq 0.02$; NS, no significant difference (Kruskal–Wallis test). Total number of cells: 0-h control, 1816; 4-h control, 1511; oxytocin 0.02 test, 850; and oxytocin test 0.20 test, 750. See Supplemental Figure S6 for further details of the assay. BODIPY-stained LDs are shown in red and cytoplasmic GFP in green; adp, adipocyte; AL, alveolar lumen. Bars, 30 μm (A–D, F, H, J); 50 μm (E, G, I); 20 μm (Supplemental Video S5.mov).

Stemberger *et al.*, 1984). Thus final assembly of droplets with diameters between 4 and 10 μm, which account for the bulk volume of secreted milk lipid (Supplemental Figure S1, C and D), may occur outside the confines of the cytoplasm, an efficient approach for handling large volumes of lipid without compromising cell structure and the secretory apparatus.

The slow formation of LDs associated with the plasma membrane resolves the long-standing paradox that although multiple intracellular membranes may associate with droplets in the cell (Wooding, 1971; Peixoto de Menezes and Pinto da Silva, 1979; Wu *et al.*, 2000; Honvo-Houéto *et al.*, 2016), the outer bilayer membrane of the secreted droplets has a composition consistent with a plasma membrane origin for many of the protein and lipid constituents (Keenan *et al.*, 1970; Mather and Keenan, 1983, 1998), other than proteins such as xanthine oxidoreductase that are required for the secretion process itself (Vorbach *et al.*, 2002; Monks *et al.*, 2016). Thus, as the LD engages with the plasma membrane, apical constituents such as MUC1 (Mather *et al.*, 2001) and sphingomyelin (Keenan and Morre, 1970; Keenan *et al.*, 1970; van Meer, 1989) will gradually predominate as they intermix with proteins and lipids from intracellular membranes and as the droplets slowly emerge from the cell.

Release of LDs from the cell requires sealing of the outer membrane envelope as the apposing bilayers fuse together ("pinch off") at the final point of contact. This terminal step is not dependent on droplet size, because LDs of a wide range of diameters, from <1 to >10 μm, are secreted alongside each other (Deeney *et al.*, 1985). Neither is the "pinching off" mechanism a seamless process with no loss of cell contents, because a fraction of the secreted droplets may contain cytoplasm and membrane fragments trapped between the outer membrane and core lipid (so-called cytoplasmic crescents or signets; Wooding *et al.*, 1970; Huston and Patton, 1990). These observations are consistent with our data showing that some LDs are released in an intermittent oxytocin-dependent manner and provide a mechanistic basis for the occurrence of cytoplasmic crescents in secreted LDs. Thus, after oxytocin-induced actin contractions, most of the LDs assembling at the apical surface are released at the same time regardless of size, with or without cytoplasmic inclusions. In this event, the occurrence of such inclusions should be inversely related to the secretion profile of the droplets at the time of release, with LDs protruding furthest from the cell the least likely to contain any cytoplasmic material.

The role of oxytocin in effecting the release of many LDs raises intriguing mechanistic questions. The most direct possibility is that LDs are mechanically displaced as the myoepithelium alternately relaxes and contracts. However, this is unlikely to be sufficient to expel LDs that are still partially embedded in the cytoplasm. Additional mechanical force may be generated through controlled contractions of the actin/myosin network associated with the apical plasma membrane (Amato and Loizzi, 1981; Masedunskas *et al.*, 2014), which would require the relaying of oxytocin-induced signals from the myoepithelium. Oxytocin functions through a G protein–coupled receptor, causing the release of Ca^{2+} from intracellular stores (Gimpl and Fahrenholz, 2001). This raises the possibility that a Ca^{2+} wave is propagated through electrically coupled gap junctions between the myoepithelium and secretory epithelium (Pitelka *et al.*, 1973; Berga, 1984), indirectly leading to contractions of the apical actin cortex. In this context, several studies have shown that lactation is impaired in mice that either lack or have altered expression patterns of connexins, the principal structural components of gap junctions (Plum *et al.*, 2000; Plante *et al.*, 2010; Mroue *et al.*, 2015).

In conclusion, we describe a facile method for intravital imaging of the lactating mouse mammary gland using standard confocal

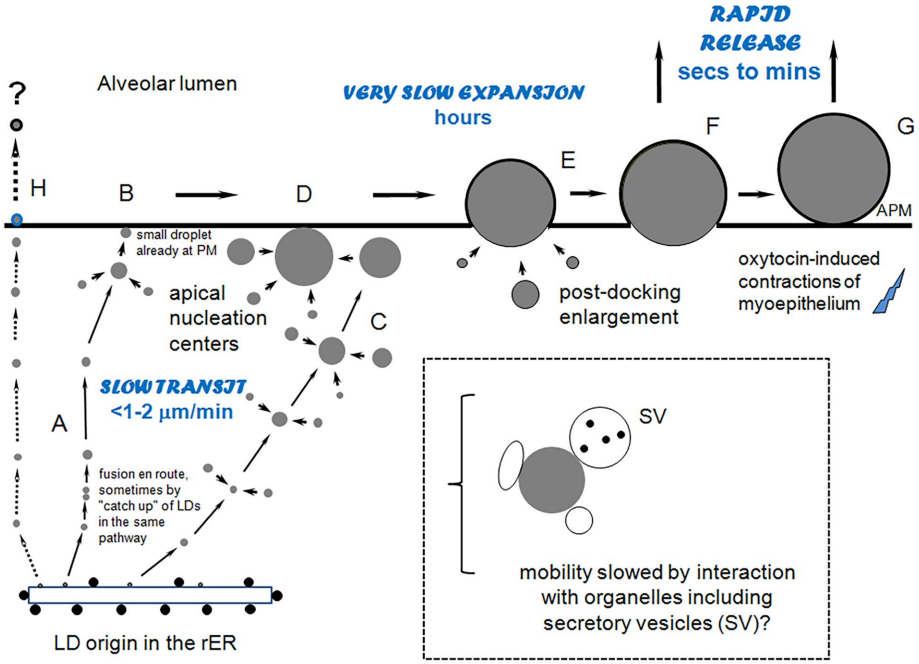

FIGURE 6: Paradigm for LD transit, growth, and release from mammary epithelial cells. (A) LDs synthesized in the rER transit to the cell apex on tracks, sometimes fusing together en route, and then fuse with a small, preexisting droplet at the apical surface (B); others expand during transit, especially in the apical cytoplasm (C) and after engaging with the apical surface (D). LD movement is slow (on the order of <1–2 µm/min), possibly because of interactions with organelles, as shown (dashed box). Droplet expansion may continue as the LDs are emerging from the cell (E), a process that can take hours. Accumulated droplets are rapidly released after oxytocin-mediated contraction of the myoepithelium, whether they are still partly associated with the cytoplasm (F) or loosely bound to the outer surface (G). Many small droplets (<1 µm) are assumed to be directly secreted from the apical surface with minimal enlargement (H). APM, apical plasma membrane.

microscopy. These techniques will have general application for investigating the assembly and secretion of milk constituents synthesized de novo in the secretory epithelium and the trafficking of preformed serosal components, such as immunoglobulins, across the mammary barrier into milk.

MATERIALS AND METHODS

Materials

BODIPY 665/676 and LipidTox FR were purchased from ThermoFisher Scientific (Invitrogen), ketamine from Putney (Portland, ME), and xylazine from MWI (Boise, ID). Synthetic oxytocin was from Sigma Chemical (St. Louis, MO).

Animal care and strains

Transgenic mouse strains used in this study were the green fluorescent FvB mouse of Hadjantonakis *et al.* (1998), in which GFP is expressed as a soluble protein in the cytosol of most cells (denoted here GFPcyto) and the C57BL/6J mTomato (*m*T/*m*G) mouse, a double fluorescent Cre reporter strain that respectively expresses either Tomato dimer or GFP before or after Cre-mediated excision of the mTomato gene (Mazumdar *et al.*, 2007). In the mTomato mouse, either fluorophore is targeted to the plasma membrane of most cells through a short sorting motif derived from the MARCKS protein. For this study, the mTomato mouse was bred to the CMV-Cre mouse to generate GFP-membrane progeny.

Mice were bred one pair per cage and maintained on standard mouse chow and water ad libitum. The first day of lactation was counted as day 1, and mice were analyzed at midlactation between days 9 and 11 for all procedures (milking, imaging, and fluorescence microscopy of fixed tissue). All surgical techniques and imaging procedures under anesthesia were approved by the National Institutes of Health Institutional Animal Care and Use Committee.

Intravital imaging

Mice were anesthetized with 3.5% isoflurane for 5 min, followed by i.p. injection of a mixture of xylazine and ketamine (~15 and 100 mg/kg body weight, respectively). A deep plane of anesthesia was then maintained throughout the whole procedure by follow-up doses of xylazine or ketamine administered by i.p. or subcutaneous injection. Animals were checked for an adequate level of anesthesia every 10–20 min through palpebral and toe pinch reflexes.

Before surgery, skin surrounding the inguinal glands on the right side (in the supine position) was shaved and the animal kept warm with an overhead heating lamp. The number 4 mammary gland (Figure 1B) was exposed by making a circular incision around the gland and gently peeling away the skin from the abdomen. This created a skin flap in which the gland and associated vasculature was still attached (Figure 1C). Extraneous connective and adipose tissue was carefully removed with forceps and the abdominal wall kept moist with carbomer 940 gel and Parafilm. Any damaged blood vessels were sealed with a hand-held cauterizer and the cut surfaces rinsed with saline. LDs were labeled by repetitively bathing the exposed gland with saline containing 10 µM BODIPY 665/676 (total of 1.0 ml for ≤1 h) during surgery.

The mouse was then placed ventral-side down on a heating pad, which was mounted onto the microscope stage to keep the animal at physiological temperature. The skin flap was then spread out onto the premoistened microscope stage (Figure 1D), and any exposed cut surfaces were protected from dehydration by coating with carbomer 940 gel. The gland was isolated from body movements by placing a custom-made barrier between the abdominal wall and the glass coverslip attached to the stage insert and the rear leg and tail immobilized with sticky tape. A Plexiglas sheet was then placed on top of the skin flap and secured with tape to prevent the gland from slipping on the glass surface during imaging. Finally, the animal was covered with layers of gauze for warmth (Figure 1E). For successful imaging, the two most important goals were to achieve maximum stability with minimal pressure on the gland and associated vasculature. Capillary blood flow was monitored throughout the procedure by fluorescence microscopy to ensure optimal conditions for imaging.

Images were acquired with an Olympus FluoView 1000 Confocal Microscope (Olympus America) equipped with a 60x PLAPON oil immersion objective (NA 1.42) preheated to 37°C to avoid thermal aberrations. GFP was excited at 488 nm and the fluorescence emission collected at 560 nm using a BA 505–605 band-pass filter. BODIPY 665/676 was excited at 633 nm and the emission collected at 668 nm using a BA 655–755 band-pass filter. Line-scan images

were acquired at scan speeds of either 4 or 8 µs/pixel (512 × 512 pixels; 12 bits per pixel) every 5 or 10 s for 1–2 h. Images were stored as TIFF files and converted into movies using MetaMorph (Molecular Devices) and ImageJ (National Institutes of Health) software. For further information on the technical aspects of intravital imaging of solid tissues, see Masedunskas *et al.* (2014).

Quantitative analysis of movies

Three GFPcyto mice at midlactation (day 9 or 10) nursing eight pups each were used to generate 1- or 2-h movies as described earlier. Each movie was subdivided into three or four regions of interest (e.g., Figure 2D) and LD motion evaluated either through a customized program (Matlab) or by manual tracking.

For the customized program, BODIPY-stained LDs were segmented using the autoshredding function in ImageJ. A manually drawn outline of the apical plasma membrane was used as the ultimate frame of reference for defining the direction of movement. The *XY*-coordinates of the LD centroid were determined and recorded to generate the trajectory of the LD over time. The *XY*-coordinates along the LD perimeter were recorded and used to find the shortest distance between the LD and the apical plasma membrane. The distance was documented in every frame for subsequent dynamic analysis. This program was useful for estimating short-term (+/–) motion (Table 1) frame by frame (5 or 10 s/frame) and for analyzing in detail the trajectories of selected LDs (e.g., Supplemental Figure S2). However, over time, there was a significant drift in some areas of the movies relative to the manually drawn frame of reference, which compromised a comprehensive meta-analysis.

To obtain semiquantitative data, the same movies were reanalyzed by manually tracking 300 LDs using Fiji (National Institutes of Health). Altogether 300 LDs in all positions in the cells were tracked frame by frame in the most stable regions (~100 LDs per mouse). The beginning and end positions of each LD in the cell were measured as the shortest perpendicular distance from the LD to the apical surface and the total distances traveled (anything from 0 to 10 µm) estimated as a straight line between the initial and final positions. The problem of measuring LD volume (a 3D parameter) in two-dimensional (2D) movies was addressed by using the largest 2D area for each droplet observed within the first 1–2 min. This assumes that there is sufficient mobility in the *Z*-dimension within this time to reveal the maximum diameter of each droplet, a reasonable assumption for LDs ≤3.6 µm in diameter, as the confocal slice thickness was set to 1.2 µm. Thus, because of this restriction, the sizes of LDs >3.6 µm should be regarded as minimal estimates. In a second iteration, only the most extensive and contiguous mobile portion of each track was analyzed to estimate maximum droplet speeds. All measurements were recorded in triplicate. MSDs were calculated using the formula $<r^2> = (x - x_0)^2 + (y - y_0)^2$, where r represents MSD, x and y represent the *X*- and *Y*-coordinates of the LD centroid in the current frame, and x_0 and y_0 represent the *X*- and *Y*-coordinates of the LD centroid in the first frame. The mode of lateral mobility was determined by the shape of the MSD curve via visual inspection, where the MSD curve of the diffusive mode appears to be a straight line, the directed (superdiffusive) mode a hyperbolic curve, and the mixed mode a curve containing both diffusive and directed modes in a fragmented manner (Chen *et al.*, 2006).

Collection of mouse milk

GFP-membrane mice (day 10 lactation) were separated from their litters for 4 h, anesthetized by exposure to 3.0–3.5% isoflurane, and injected with 0.2 IU of oxytocin to stimulate milk let-down. Milk was collected into standard glass-bore tubes with a hand-held milking device connected to a vacuum pump and immediately transferred into capillary tubes to avoid evaporative losses (Teter *et al.*, 1990).

Chemical fixation of lactating mammary tissue

GFP-membrane mice (day 10 lactation) were anesthetized with 3.5% isoflurane for 5 min, followed by the i.p. injection of a mixture of xylazine and ketamine (–20 and 100 mg/kg body weight, respectively). Glands were fixed at room temperature by intracardiac whole-body perfusion of 4% paraformaldehyde in 0.1 M phosphate buffer, pH 7.2, and the dissected number 4 glands stored at 4°C in fixative.

Confocal microscopy of milk and lactating mammary gland

Milk. LDs in freshly collected milk were immediately labeled with BODIPY 665/676 by adding a 10 mM stock solution (stored frozen in dimethyl sulfoxide) to the whole-milk samples to a final concentration of 10 µM at room temperature. After incubation at room temperature for 30 min, drops of the labeled milk were placed on microscope slides and sealed under coverslips for immediate imaging.

LDs were examined by confocal microscopy essentially as described under *Intravital imaging* using the 60× oil immersion objective. Optical *Z*-sections (0.5 µm) were obtained at a speed of 8 µs/pixel by line scan (640 × 640 pixels; 12 bits/pixel) to a depth of 20 µm for 3D reconstructions and image analysis. Four such randomly chosen 3D reconstructions per mouse ($n = 3$) were used to estimate LD frequency and volume using Imaris (Bitplane) software (total number of LDs, 14,298; Supplemental Figure S1, C and D).

Tissue. Paraformaldehyde-fixed mammary tissue was embedded in low–melting point agarose and cut into 100-µm sections with a Leica Series 1000 vibratome. Sections were stained with LipidTox FR (200× dilution of commercial stock) in phosphate-buffered saline (PBS) at room temperature for 30 min, rinsed with PBS, and mounted on microscope slides in VectaShield mounting medium with or without 4′,6-diamidino-2-phenylindole (DAPI).

For estimation of LD numbers and sizes in the GFP-membrane mouse (Supplemental Figure S1, A and B), 3D reconstructions from confocal sections were generated as described for milk samples, except that the frame size was 512 × 512 pixels and DAPI-stained nuclei were detected by excitation at 405 nm, with fluorescence emission collected between 430 and 460 nm. Cell numbers were estimated by counting DAPI-stained nuclei. Cells with double nuclei (Rios, Fu, *et al.*, 2016) were identified by using the GFP-labeled plasma membranes to trace the outer limits of each cell. Four 3D reconstructions per mouse ($n = 3$) were used to estimate LD frequency and volume (total of 362 cells, 10,398 LDs, 28.7 LDs/cell).

To estimate the amount of lipid associated with the apical plasma membrane in the GFPcyto mouse (Figure 5K), two sections each from the number 4 glands (right and left) were stained with LipidTox FR, and eight 3D reconstructions/mouse (512 × 512) were generated as described. Apical LDs that were still partially associated with the cytoplasm were identified by scanning through a standard depth of 10 µm (20 optical sections), and the volume of each droplet was estimated from the diameters. Droplets were included in the analysis if they protruded by at least 30% from the cell in maximal *X*/*Y* profile, a fraction of the BODIPY-stained lipid was in contact with the GFP-labeled cytoplasm, and the droplet diameter was ≥1 µm. LDs that were maximally protruding from the cell with no obvious contact with the cytoplasm were excluded (see Supplemental Figure S6 for a complete description). Mice at 9–11 d of lactation and nursing 8–10 pups each were immediately separated from their litters and

perfusion fixed for analysis (0-h control, $n = 4$), separated from their litters for 4 h before being killed (4-h control, $n = 4$), or separated from their litters for 4 h, anesthetized, and then injected with oxytocin (either 0.02 IU [oxytocin 0.02 test, $n = 2$] or 0.20 IU [oxytocin 0.20 test, $n = 2$]), left for 20 min, and then perfusion fixed for analysis (total number of cells: 0-h control, 1816; 4-h control, 1511; oxytocin 0.02 test, 850; oxytocin 0.20 test, 750).

Statistical analysis

Data were analyzed for significance using either the Tukey and Kramer or Kruskal–Wallis tests in R (R Development Core Team, 2014), as indicated in the text.

ACKNOWLEDGMENTS

We thank Muhibullah Tora and Olivia Harding for help with animal care, Li Ma (Department of Animal and Avian Sciences, University of Maryland) for advice with the statistical analysis, and Wei-Hung Jung (Department of Mechanical Engineering, Johns Hopkins University) for help with MSD analysis. This research was supported by the Intramural Research Program of the National Institutes of Health, National Cancer Institute, Center for Cancer Research, and the National Institute of Dental and Craniofacial Research. I.H.M. was funded in part by the Maryland Agricultural Experiment Station and grants from the U.S. Department of Agriculture National Research Initiative Program (2005–04637) and National Institute of Child Health and Human Development, National Institutes of Health (1R01 HD048588-01A1).

REFERENCES

Boldface names denote co–first authors.

Amato PA, Loizzi RF (1981). The identification and localization of actin and actin-like filaments in lactating guinea pig mammary gland alveolar cells. Cell Motil 1, 329–347.

Bargmann W, Knoop A (1959). Über die Morphologie der Milchsekretion. Licht- und Elektronenmikroskopische Studien an der Milchdrüse der Ratte. Z Zellforsch 49, 344–388.

Barneda D, Planas-Iglesias J, Gaspar ML, Mohammadyani4 D, Prasannan S, Dormann D, Han G-S, Jesch SA, Carman GM, Kagan V, *et al.* (2015). The brown adipocyte protein CIDEA promotes lipid droplet fusion via a phosphatidic acid-binding amphipathic helix. Elife 4, e07485.

Berga SE (1984). Electrical potentials and cell-to-cell dye movement in mouse mammary gland during lactation. Am J Physiol 247, C20–C25.

Caspi A, Granek R, Elbaum M (2000). Enhanced diffusion in active intracellular transport. Phys Rev Lett 85, 5655–5658.

Chen Y, Lagerholm BC, Yang B, Jacobson K (2006). Methods to measure the lateral diffusion of membrane lipids and proteins. Methods 39, 147–153.

Chong BM, Reigan P, Mayle-Combs KD, Orlicky DJ, McManaman JL (2011). Determinants of adipophilin function in milk lipid formation and secretion. Trends Endocrinol Metab 22, 211–217.

Deeney JT, Valivullah HM, Dapper CH, Dylewski DP, Keenan TW (1985). Microlipid droplets in milk secreting mammary epithelial cells: evidence that they originate from endoplasmic reticulum and are precursors of milk lipid globules. Eur J Cell Biol 38, 16–26.

Dutta A, Sinha DK (2015). Turnover of the actomyosin complex in zebrafish embryos directs geometric remodelling and the recruitment of lipid droplets. Sci Rep 5, 13915.

Dylewski DP, Dapper CH, Valivullah HM, Deeney JT, Keenan TW (1984). Morphological and biochemical characterization of possible intracellular precursors of milk lipid globules. Eur J Cell Biol 35, 99–111.

Dylewski DP, Keenan TW (1984). Centrioles in the mammary epithelium of the rat. J Cell Sci 72, 185–193.

Franke WW, Heid HW, Grund C, Winter S, Freudenstein C, Schmid E, Jarasch E-D, Keenan TW (1981). Antibodies to the major insoluble milk fat globule membrane-associated protein: specific location in apical regions of lactating epithelial cells. J Cell Biol 89, 485–494.

Fujimoto Y, Itabe H, Kinoshita T, Homma KJ, Onoduka J, Mori M, Yamaguchi S, Makita M, Higashi Y, Yamashita A, Takano T (2007). Involvement of ACSL in local synthesis of neutral lipids in cytoplasmic lipid droplets in human hepatocyte HuH7. J Lipid Res 48, 1280–1292.

Gimpl G, Fahrenholz F (2001). The oxytocin receptor system: structure, function, and regulation. Physiol Rev 81, 629–683.

Gong J, Sun Z, Wu L, Xu W, Schieber N, Xu D, Shui G, Yang H, Parton RG, Li P (2011). Fsp27 promotes lipid droplet growth by lipid exchange and transfer at lipid droplet contact sites. J Cell Biol 195, 953–963.

Gorden PJ, Timms LL (2004). Lactation. In: Dukes' Physiology of Domestic Animals, ed. WO Reece, Ithaca, NY: Cornell University Press, 694–714.

Gouon-Evans V, Lin EY, Pollard JW (2002). Requirement of macrophages and eosinophils and their cytokines/chemokines for mammary gland development. Breast Cancer Res 4, 155–164.

Hadjantonakis AK, Gertsenstein M, Ikawa M, Okabe M, Nagy A (1998). Generating green fluorescent mice by germline transmission of green fluorescent ES cells. Mech Dev 76, 79–90.

Head JH, Beer AE (1978). The immunologic role of viable leukocytic cells in mammary exosecretions. In: Lactation, A Comprehensive Treatise, Vol. IV, ed. BL Larson, New York: Academic Press, 337–364.

Heid HW, Keenan TW (2005). Intracellular origin and secretion of milk fat globules. Eur J Cell Biol 84, 245–258.

Honvo-Houéto E, Henry C, Chat S, Layani S, Truchet S (2016). The endoplasmic reticulum and casein-containing vesicles contribute to milk fat globule membrane. Mol Biol Cell 27, 2946–2964.

Huston GE, Patton S (1990). Factors related to the formation of cytoplasmic crescents on milk fat globules. J Dairy Sci 73, 2061–2066.

Innis SM (1991). Essential fatty acids in growth and development. Prog Lipid Res 30, 39–103.

Jack LJW, Mather IH (1990). Cloning and analysis of cDNA encoding bovine butyrophilin, an apical glycoprotein expressed in mammary tissue and secreted in association with the milk-fat globule membrane during lactation. J Biol Chem 265, 14481–14486.

Jeong J, Lisinski I, Kadegowda AKG, Shin H, Wooding FBP, Daniels BR, Schaack J, Mather IH (2013). A test of current models for the mechanism of milk-lipid droplet secretion. Traffic 14, 974–986.

Jeong J, Rao AU, Xu J, Ogg SL, Hathout Y, Fenselau C, Mather IH (2009). The PRY/SRY/B30.2 domain of butyrophilin 1a1 (Btn1a1) binds to xanthine oxidoreductase: implications for the function of Btn1a1 in the mammary gland and other tissues. J Biol Chem 284, 22444–22456.

Kassan A, Herms A, Fernández-Vidal A, Bosch M, Schieber NL, Reddy BJN, Fajardo A, Gelabert-Baldrich M, Tebar F, Enrich C, *et al.* (2013). Acyl-CoA synthetase 3 promotes lipid droplet biogenesis in ER microdomains. J Cell Biol 203, 985–1001.

Keenan TW, Morré DJ (1970). Phospholipid class and fatty acid composition of Golgi apparatus isolated from rat liver and comparison with other cell fractions. Biochemistry 9, 19–25.

Keenan TW, Morré DJ, Olson DE, Yunghans WN, Patton S (1970). Biochemical and morphological comparison of plasma membrane and milk fat globule membrane from bovine mammary gland. J Cell Biol 44, 80–93.

Knight CH, Maltz E, Docherty AH (1986). Milk yield and composition in mice: effects of litter size and lactation number. Comp Biochem Physiol 84A, 127–133.

Knoblach B, Rachubinski RA (2015). Transport and retention mechanisms govern lipid droplet inheritance in *Saccharomyces cerevisiae*. Traffic 16, 298–309.

Larque E, Demmelmar H, Koletzko B (2002). Perinatal supply and metabolism of long-chain polyunsaturated fatty acids: Importance for the early development of the nervous system. Ann NY Acad Sci 967, 299–310.

Martin S, Parton RG (2006). Lipid droplets: a unified view of a dynamic organelle. Nat Rev Mol Cell Biol 7, 373–378.

Masedunskas A, Weigert R, Mather IH (2014). Intravital imaging of the lactating mammary gland in transgenic mice expressing fluorescent proteins. In: Advances in Intravital Microscopy, ed. R Weigert, Dordrecht, Netherlands: Springer-Verlag, 187–204.

Mather IH, Jack LJW, Madara PJ, Johnson VG (2001). The distribution of MUC1, an apical membrane glycoprotein, in mammary epithelial cells at the resolution of the electron microscope: implications for the mechanism of milk secretion. Cell Tissue Res 304, 91–101.

Mather IH, Keenan TW (1983). Function of endomembranes and the cell surface in the secretion of organic milk constituents. In: Biochemistry of Lactation, ed. TB Mepham, Amsterdam: Elsevier, 231–283.

Mather IH, Keenan TW (1998). Origin and secretion of milk lipids. J Mammary Gland Biol Neoplasia 3, 259–273.

Maucort G, Kasula R, Papadopulos A, Nieminen TA, Rubinsztein-Dunlop H, Meunier FA (2014). Mapping organelle motion reveals a vesicular conveyor belt spatially replenishing secretory vesicles in stimulated chromaffin cells. PLoS One 9, e87242.
Mazumdar MD, Tasic B, Miyamichi K, Li L, Luo L (2007). A global double-fluorescent Cre reporter mouse. Genesis 45, 593–605.
McManaman JL (2012). Milk lipid secretion: recent biomolecular aspects. Biomol Concepts 3, 581–591.
McManaman JL, Russell TD, Schaack J, Orlicky DJ, Robenek H (2007). Molecular determinants of milk lipid secretion. J Mammary Gland Biol Neoplasia 12, 259–268.
Monks J, Dzieciatkowska M, Bales ES, Orlicky DJ, Wright RM, McManaman JL (2016). Xanthine oxidoreductase mediates membrane docking of milk-lipid droplets but is not essential for apocrine milk fat globule secretion. J Physiol 594, 5899–5921.
Moriya H, Uchida K, Okajima T, Matsuda T, Nadano D (2011). Secretion of three enzymes for fatty acid synthesis into mouse milk in association with fat globules, and rapid decrease of the secreted enzymes by treatment with rapamycin. Arch Biochem Biophys 508, 87–92.
Mroue R, Inman J, Mott J, Budunova I, Bissell MJ (2015). Asymmetric expression of connexins between luminal epithelial- and myoepithelial-cells is essential for contractile function of the mammary gland. Dev Biol 399, 15–26.
Murphy DJ (2001). The biogenesis and functions of lipid bodies in animals, plants and microorganisms. Prog Lipid Res 40, 325–438.
Oftedal OT (1984). Milk composition, milk yield and energy output at peak lactation: a comparative review. Symp Zool Soc Lond 51, 33–85.
Oftedal OT, Iverson SJ (1995). Comparative analysis of nonhuman milks. Phylogenetic variation in the gross composition of milks. In: Handbook of Milk Composition, ed. RG Jensen, New York: Academic Press, 749–789.
Ogg SL, Weldon AK, Dobbie L, Smith AJH, Mather IH (2004). Expression of butyrophilin (Btn1a1) in lactating mammary gland is essential for the regulated secretion of milk-lipid droplets. Proc Natl Acad Sci USA 101, 10084–10089.
Peixoto de Menezes A, Pinto da Silva P (1979). Fat droplet formation in rat lactating mammary gland and mammary carcinomas viewed by freeze-fracture. Lab Invest 40, 545–553.
Pitelka DR, Hamamoto ST, Duafala JG, Nemanic MK (1973). Cell contacts in the mouse mammary gland I. Normal gland in postnatal development and the secretory cycle. J Cell Biol 56, 797–818.
Plante I, Wallis A, Shao Q, Laird DW (2010). Milk secretion and ejection are impaired in the mammary gland of mice harboring a Cx43 mutant while expression and localization of tight and adherens junction proteins remain unchanged. Biol Reprod 82, 837–847.
Plum A, Hallas G, Magin T, Dombrowski F, Hagendorff A, Schumacher B, Wolpert C, Kim J-S, Lamers WH, Evert M, *et al*. (2000). Unique and shared functions of different connexins in mice. Curr Biol 10, 1083–1091.
R Development Core Team (2014). R: A Language and Environment for Statistical Computing. Version 3.1.1. Available at http://www.R-project.org/ (accessed 10 July 2014).
Reed JR, Schwertfeger KL (2010). Immune cell location and function during post-natal mammary gland development. J Mammary Gland Biol Neoplasia 15, 329–339.
Reverey JF, Jeon J-H, Bao H, Leippe M, Metzler R, Selhuber-Unkel C (2015). Superdiffusion dominates intracellular particle motion in the supercrowded cytoplasm of pathogenic Acanthamoeba castellanii. Sci Rep 5, 11690.
Rios AC, Fu NY, Jamieson PR, Pal B, Whitehead L, Nicholas KR, Lindeman GJ, Visvader JE (2016). Essential role for a novel population of binucleated mammary epithelial cells in lactation. Nat Commun 7, 11400.
Stemberger BH, Patton S (1981). Relationship of size, intracellular location, and time required for secretion of milk fat droplets. J Dairy Sci 64, 422–426.
Stemberger BH, Walsh RM, Patton S (1984). Morphometric evaluation of lipid droplet associations with secretory vesicles, mitochondria and other components in the lactating cell. Cell Tissue Res 236, 471–475.
Suzuki M, Shinohara Y, Ohsaki Y, Fujimoto T (2011). Lipid droplets: size matters. J Electron Microsc (Tokyo) 60, S101–S116.
Targett-Adams P, Chambers D, Gledhill S, Hope RG, Coy JF, Girod A, McLauchlan J (2003). Live cell analysis and targeting of the lipid droplet-binding adipocyte differentiation-related protein. J Biol Chem 278, 15998–16007.
Tauchi-Sato K, Ozeki S, Houjou T, Taguchi R, Fujimoto T (2002). The surface of lipid droplets is a phospholipid monolayer with a unique fatty acid composition. J Biol Chem 277, 44507–44512.
Teter BB, Sampugna J, Keeney M (1990). Milk fat depression in C57Bl/6J mice consuming partially hydrogenated fat. J Nutr 120, 818–824.
van Meer G (1989). Lipid traffic in animal cells. Annu Rev Cell Biol 5, 247–275.
Vorbach C, Scriven A, Capecchi MR (2002). The housekeeping gene xanthine oxidoreductase is necessary for milk fat droplet enveloping and secretion: gene sharing in the lactating mammary gland. Genes Dev 16, 3223–3235.
Wang W, Lv N, Zhang S, Shui G, Qian H, Zhang J, Chen Y, Ye J, Xie Y, Shen Y, *et al.* (2012). Cidea is an essential transcriptional coactivator regulating mammary gland secretion of milk lipids. Nat Med 18, 235–243.
Weigert R, Porat-Shliom N, Amornphimoltham P (2013). Imaging cell biology in live animals: ready for prime time. J Cell Biol 201, 969–979.
Welte MA (2009). Fat on the move: intracellular motion of lipid droplets. Biochem Soc Trans 37, 991–996.
Welte MA, Gross SP, Postner M, Block SM, Wieschaus EF (1998). Developmental regulation of vesicle transport in *Drosophila* embryos: forces and kinetics. Cell 92, 547–557.
Wilfling F, Haas JT, Walther TC, Farese RV Jr (2014). Lipid droplet biogenesis. Curr Opin Cell Biol 29, 39–45.
Wooding FBP (1971). The mechanism of secretion of the milk fat globule. J Cell Sci 9, 805–821.
Wooding FBP (1977). Comparative mammary fine structure. Symp Zool Soc Lond 41, 1–41.
Wooding FBP, Peaker M, Linzell JL (1970). Theories of milk secretion: evidence from the electron microscopic examination of milk. Nature 226, 762–764.
Wu CC, Howell KE, Neville MC, Yates JR 3rd, McManaman JL (2000). Proteomics reveal a link between the endoplasmic reticulum and lipid secretory mechanisms in mammary epithelial cells. Electrophoresis 21, 3470–3482.